Active Thermal Control optimization and evaluation with detailed simulation and different lifetime models

Downloaded from: https://research.chalmers.se, 2026-05-21 19:12 UTC

Citation for the original published paper (version of record):

Brzycki, M., Sharma, N., Lai, L. et al (2025). Active Thermal Control optimization and evaluation with detailed simulation and different
lifetime models. IECON Proceedings (Industrial Electronics Conference): 1-7.
http://dx.doi.org/10.1109/IECON58223.2025.11221919

N.B. When citing this work, cite the original published paper.

© 2025 IEEE. Personal use of this material is permitted. Permission from IEEE must be obtained for all other uses, in any current or future media, including reprinting/republishing this material for advertising or promotional purposes, or reuse of any copyrighted component of this work in other works.

(article starts on next page)

Active Thermal Control optimization and evaluation with detailed simulation and different lifetime models

Maciej Brzycki
Electrical Engineering Department
Chalmers University of Technology
Gothenburg, Sweden
brzycki@chalmers.se

Nimananda Sharma
Volvo group
Gothenburg, Sweden
nimananda.sharma.2
@volvo.com

Linhua Lai
Electrical Engineering Department
Chalmers University of Technology
Gothenburg, Sweden
linhua@chalmers.se

Artem Rodionov
Electrical Engineering Department
Chalmers University of Technology
Gothenburg, Sweden
artem@chalmers.se

Yujing Liu
Electrical Engineering Department
Chalmers University of Technology
Gothenburg, Sweden
yujing.liu@chalmers.se

***Abstract* - Silicon carbide (SiC) power semiconductors are superior to traditional silicon devices due to their higher efficiency and performance, but face challenges related to temperature swings caused by very low thermal capacity, which limits their lifespan. To address this issue, this study proposes control methods to regulate the junction temperature of the SiC devices to reduce temperature swings also referred to as Active Thermal Control (ATC). This approach reduces temperature swings, thereby extending the lifetime of SiC devices. The article focuses on the practical meaning of the implementation of thermal management – main goal is to present advantages from system perspective, that can be gained in terms of longer life expectancy by reducing thermal stresses. The benefits were evaluated using a high-precision simulation model with a small timestep, enabling analysis of transistor switching and temperature transients. Results showed that implementing even a simple temperature management algorithm, without any changes to the hardware, provides measurable benefits.**

Keywords - silicon carbide (SiC) inverter, active thermal control (ATC), remaining useful lifetime (RUL), lifetime prediction, power cycling, reliability

I. INTRODUCTION

The global adoption of electric vehicles (EVs) is on the rise, driven by environmental concerns and technological advancements. Power semiconductors are crucial to the operation of EVs, serving as key components in vital powertrain systems such as inverters, battery management systems, and chargers. Automakers are increasingly focusing on advanced technologies such as wide band gap devices like silicon carbide (SiC) and gallium nitride (GaN) with integrated drive topologies to enhance performance, lower mass, and reduce costs [1]. Along with striving to increase power density and reduce size, more significant thermal management problems may occur. The reduction in component size and thus smaller heat transfer area, negatively affects the heat dissipation capabilities. This results in higher junction temperatures, which can affect the lifespan of the power semiconductors [2]. Moreover, reducing size of the entire system, including heat sinks, decreases the total heat capacity – and thus significantly increases the temperature difference (ΔT_j) during a cycle. Continuous heating and cooling (thermal cycling) applies thermomechanical strain to the material layers [3].

Studies indicate that thermal cycling and resulting strains are primary factors in the accelerated deterioration which occurs due to frequent changes in the load current [4] and transistor switching. Because of the different thermal expansion coefficients of interfacing materials, failures commonly occur at the point of contact [5]. The most frequent thermally induced failure modes at the package level of semiconductor are bond wire lift-off and solder joint breakage [6], [7]. The vulnerability of these parts to failure due to thermal cycling necessitates a solution. One way of solving this problem is to actively control junction temperature during operation, which is the focus of this research and is referred to as active thermal control techniques (ATC). Studies on failure cycles and lifetime modeling suggest that large temperature swings reduce semiconductor lifespan more significantly than continuous operation at a higher mean junction temperature T_J [8], [9]. Different active thermal control strategies are explored in the literature [10]. In general, we can divide these methods into two different approaches - manipulation of losses or heat dissipation. Many of these methods require additional hardware modifications, making implementation on existing systems complex and costly. Moreover, strategies like load current control and modulation coefficient control increase overall control complexity. A relatively simpler alternative - adjusting transistor switching frequency, has been suggested [11], [12], [13]. However, its effectiveness in mitigating temperature-induced failures, its impact on overall SiC inverter system performance and the optimization of ATC systems, remain insufficiently explored.

Existing studies on ATC typically validate their approaches using only a single semiconductor lifetime model, which limits the ability to generalize conclusions. Since different lifetime models vary significantly due to differences in parameter conditions, device characteristics, and modeling approaches, relying on just one model may overlook key insights. Furthermore, prior research often focuses on the benefits of ATC without thoroughly analyzing its potential drawbacks, such as inverter current distortion caused by switching frequency adjustments. To address these gaps, this study evaluates ATC

This research has received funding from the EU's Horizon Europe research and innovation program EU MSCA DN under grant agreement no. 101072580, HIPO: Integrated high-speed power systems for industry and mobile applications. The content of this publication does not reflect the official opinion of the EU. Responsibility for the information and views expressed in the publication lies entirely with the authors.

strategies across three different lifetime models, helping to identify mutual trends. Additionally, the high-precision, short-timestep model enables a more comprehensive understanding of both benefits and possible trade-offs of ATC. Detailed approach facilitates implementation by enabling pre-optimization of crucial control parameters (e.g. switching frequency range).

In this article, at first, an analytical modeling of semiconductor conduction and switching losses is presented in section II. It is followed by the description of junction temperature estimation and the active thermal control method used. Section III describes the lifetime model of the semiconductor and lifetime estimation with quantitative analysis using Rainflow method. Section IV presents results, sensitivity analysis for three lifetime models and achievable lifetime extensions with different control parameters and system optimization.

II. Loss Modelling, Junction Temperature Estimation and Active Thermal Control

Junction temperature measurement is crucial to ensure effective thermal management. This value can be obtained with direct methods or estimations. Direct methods, despite their high accuracy, have several drawbacks. For example, optical measurement requires an optical connection to the semiconductor, which prevents the use of common dielectric gel [14]. On the other hand, contact measurement introduces non-negligible delay. Utilizing a model-based approach, the thermal response time of the physical system and measurement circuits can be omitted, enabling predictive control behavior.

A. Loss Modelling

Effective thermal management of transistors is based on accurately estimating power losses during conduction and switching period. Conduction losses occur in both transistor and reverse diode. However, the majority of these losses is caused by the voltage drop on essential SiC transistor parameter - on-state drain source resistance R_{on}.

$$P_{\mathrm{c,M+D}} = \frac{1}{T_{\mathrm{sw}}}\int_0^{T_{\mathrm{sw}}}\left[V_{\mathrm{fd}} i_f(t) + R_{\mathrm{fd}} i_f(t) + R_{\mathrm{on}} {i_d}^2(t)\right]dt \quad (1)$$

Average losses in three-phase two-level inverter per one period with SVPWM modulation can be calculated based on peak current (I_{m}), modulation coefficients (M), parallel conduction angle (β) and power factor ($\cos\varphi$). The general formula for conducting losses in single SiC transistor is [15]:

$$\begin{aligned} P_{c,T} = {} & \frac{R_{\mathrm{on}} I_{\mathrm{m}}^2}{4\pi}\cdot(AB + CD) \\ & + \frac{R_{\mathrm{on}} I_{\mathrm{m}}^2}{4\pi(R_{\mathrm{on}} + R_{\mathrm{fd}})^2}\cdot\Big(R_{\mathrm{fd}}^2 I_m^2\cdot(A\pi - B\pi - CD) \\ & + V_{\mathrm{fd}}^2\big((\pi - 2\beta)A - D\cos(\beta)\big) \\ & + I_{\mathrm{m}}^2 R_{\mathrm{fd}} V_{\mathrm{fd}}(4A\cos(\beta) - D\pi + BD)\Big) \quad (2) \end{aligned}$$

where:

$$\begin{cases} A = 1 - 2t_{\mathrm{bl}} f_{\mathrm{sw}} \quad (3) & B = \dfrac{\pi}{2} + \beta - \dfrac{\sin(2\beta)}{2} \quad (4) \\ C = \cos(\beta) - \dfrac{\cos^2(\beta)}{3} \quad (5) & D = 2M\cos(\varphi) \quad (6) \end{cases}$$

Reverse diode conducts only in the situation where voltage drop on the SiC transistor will be higher than forward voltage of a diode:

$$\sin(\beta) = \frac{V_{\mathrm{fd}}}{R_{\mathrm{on}} I_{\mathrm{m}}} < 1 \quad (7)$$

Because of very high forward voltage, in most applications, reverse diode rarely conducts during operation, contributing negligibly to total losses. Therefore, β angle can be assumed as equal to $\frac{1}{2}\pi$ and conducting losses formula is simplified to:

$$P_{\mathrm{c}} = \frac{R_{\mathrm{on}} I_{\mathrm{m}}^2}{4} \quad (8)$$

Switching losses in transistors occur during transition between the on-state and off-state and can be significant in high-frequency power conversion systems. They are calculated by integrating the product of the current and voltage during the switching events [16]:

$$P_{\mathrm{sw}} = \left(\frac{1}{T_{\mathrm{on}}}\int_0^{T_{\mathrm{on}}} U_d(t) i_d(t)dt + \frac{1}{T_{\mathrm{off}}}\int_0^{T_{\mathrm{off}}} U_d(t) i_d(t)dt\right)\cdot f_{\mathrm{sw}} \quad (9)$$

A simpler approach to calculating average switching losses is to use switching energy data from the transistor's datasheet (E_{on}, E_{off}), typically given for specific voltage and temperature conditions. The most common method is to employ multi-dimensional lookup tables combined with linear approximation of the loss curve. Thus, single cycle energy loss is multiplied by the number of switching events, giving the switching power loss in one transistor. Since a single transistor does not conduct throughout the entire fundamental sinewave period and drain current i_d varies, average switching losses can be calculated based on half-wave equivalent DC current:

$$I_{\mathrm{DC}} = \frac{I_{\mathrm{m}}}{\pi} \quad (10)$$

$$P_{\mathrm{sw}} = f_{\mathrm{sw}}\cdot\left(E_{\mathrm{on}(\mathrm{I_{DC}},\mathrm{U},\mathrm{T})} + E_{\mathrm{off}(\mathrm{I_{DC}},\mathrm{U},\mathrm{T})}\right) \quad (11)$$

summing up, total estimated losses of three-phase inverter are:

$$P_{\mathrm{inv}} = (P_{\mathrm{c}} + P_{\mathrm{sw}})\cdot 6 \quad (12)$$

B. Junction Temperature Estimation

Accurate estimation of the semiconductors junction temperature is possible by utilizing the calculated power losses along with the thermal characteristics of the device - thermal resistance (R_{th}) and capacitance. These parameters are used to describe the heat flow from the junction to the ambience. Typically, junction to case ($R_{\mathrm{thj\text{-}c}}$) and case to ambient ($R_{\mathrm{thc\text{-}a}}$) thermal resistances are obtained from components datasheets. Then, the steady-state temperature of all power modules with common heatsink can be calculated as [17]:

$$T_{\mathrm{j}} = T_{\mathrm{amb}} + P_{\mathrm{inv}}\cdot\left(\frac{R_{\mathrm{thj-c}}}{6} + R_{\mathrm{thc-a}}\right) \quad (13)$$

C. Active Thermal Control

The chosen method of active thermal control performs its function by controlling the switching frequency of the transistors. By adjusting the switching frequency (f_{sw}), the switching losses (P_{sw}) can be controlled, leading to changes in

junction temperature T_j (Fig. 1). Affecting total losses, this approach helps maintain a more stable junction temperature while reducing the number of high thermal cycles. The control algorithm aims to keep the estimated temperature at the same value as reference temperature value from the virtual heat sink. The core principle of the control system is to increase the switching frequency if the estimated temperature is lower than the reference temperature or decrease it when the estimated temperature rises. Implementing this control strategy reduces the number of cycles with extreme temperature difference, which are the primary contributors to transistor wear and lifespan reduction.

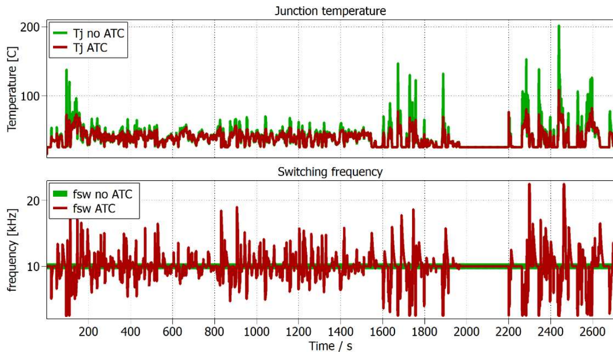

Fig. 1. Junction temperature comparison with ATC (red) and without ATC (green).

In this work, two temperature estimation signals can be distinguished. Both are calculated directly from the determined losses, multiplied by the thermal resistance. Thermal capacitance of the semiconductor can be modelled using Kalman or lowpass filter. Assuming a lower heat capacitance in the estimation than in the real object gives possibilities for predictive control and allows faster response to upcoming changes. With this approach, the estimated signal anticipates temperature changes before they actually occur, enabling the control system to react in advance. The second signal is a reference signal, additionally passed through another Kalman filter with a lower response speed. The filter emulates a virtual heat sink [3] with a higher heat capacity, which averages the temperature over a time interval (Fig. 2).

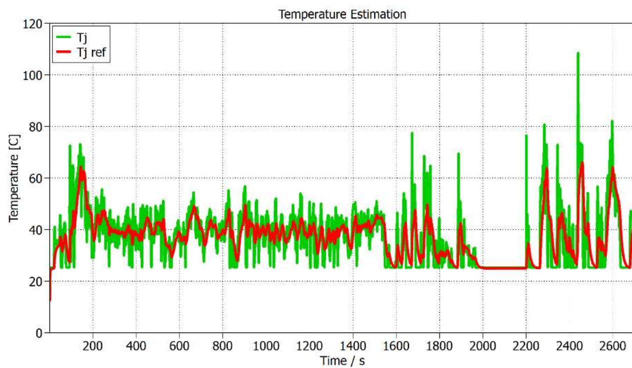

Fig. 2. Estimated temperature - no heat capacitance (green) and reference temperature with virtual heat sink capacitance (red).

For purposes of this study, only proportional controller with dead zone was implemented. Such a solution has quite a few advantages. Damping rapid changes in the response is achieved through a low-pass filter or a Kalman filter. Dead zone implementation reduces unnecessary small output changes, additionally improving stability (Fig. 3).

The use of only the proportional component in the controller ensures that the output is maintained at the same level for the same difference between T_j and $T_{j,ref}$, without the influence of the previous state. This approach keeps the average switching frequency close to a predefined nominal level, which is crucial for maintaining overall system performance. Decreasing average switching frequency can negatively affect the integrated drive system by increasing total harmonic distortion (THD) of the current generated by the inverter [18], which leads to torque ripple [19] and increased machine losses [20]. Conversely, higher switching frequency causes higher switching losses and higher copper losses caused by skin effect.

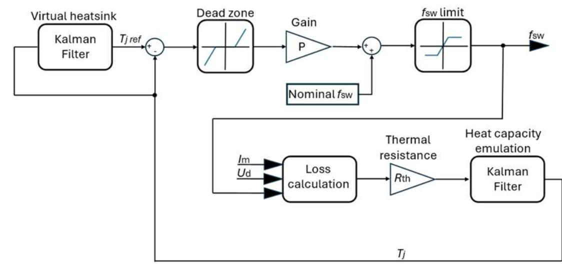

Fig. 3. ATC control schematic.

Two approaches for this ATC technique can be distinguished:

Method A sets a nominal frequency in the middle of the possible control range (or at the point of highest efficiency). In this case, the frequency can both decrease and increase during transients.

Method B sets the base switching frequency as the maximum nominal one for the system. The frequency can be only reduced when the estimated temperature increases, returning to the initial state after a certain period. Application with method B cannot respond to a decrease in temperature once a steady state at high temperature is reached. In this case, increasing the switching frequency above the nominal value to reduce the temperature change slope is not possible. The plot of frequency changes for both methods is shown in Fig. 4.

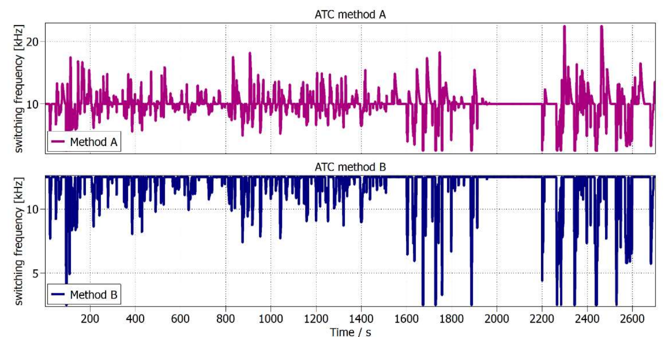

Fig. 4. Two methods of adjusting the switching frequency in ATC.

III. LIFETIME ESTIMATION

In order to evaluate the benefits of active control, methodology with remaining useful lifetime (RUL) models were used. Temperature changes are calculated based on transistor losses during example drive cycle. Then, quantitative analysis (Rainflow method) is performed on the temperature graph [21]. RUL models estimate the time to failure (in number of cycles) as a function of temperature swings (Fig. 5).

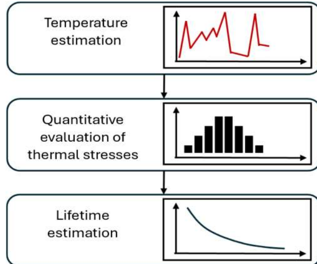

Fig. 5. Lifetime evaluation methodology.

A. Lifetime model

The most fundamental determinant of a semiconductor's lifetime is the relationship between the number of cycles to failure and thermal cycling amplitude. As thermal cycling in the real operating conditions is irregular and varies in magnitude, it is not possible to determine the lifetime curve of a semiconductor directly from it. To estimate the expected lifetime more predictably, accelerated lifetime tests - have been developed (e.g. HTGB [22], H3TRB [23], PC [24]). With these tests, carried out under uniform, stable conditions, it is possible to make an approximate estimation of the lifetime of a semiconductor during operation time. Using data from accelerated lifetime tests, semiconductor suppliers can derive empirical formulas to predict the number of cycles to failure.

General overview of the lifetime of a transistor can be obtained using commonly available models. Since the ATC method primarily aims to reduce high-amplitude thermal cycles, leading to an inevitable increase in low-amplitude cycles, it is essential to use a transistor lifetime model that is particularly accurate for small temperature swings. In this work, the primary model used is the one proposed by F. Hoffmann, S. Schmitt and N. Kaminski in [25], referred as EPE20 model.

Lifetime model formula includes several material constants β_1, β_2, θ_1, θ_2, K (Table I) and $T_{\min}$ – ambient temperature, with N_f representing the number of cycles to failure (Fig. 6).

$$N_{\mathrm{f}} = K \cdot (\Delta T_{\mathrm{j}})^{\beta_1'} \cdot e^{\left(\frac{\beta_2}{T_{\min}}\right)} \qquad (14)$$

Where β_1' is:

$$\beta_1' = e^{-\left(\frac{\Delta T_{\mathrm{j}} - \theta_1}{\theta_2}\right)} + \beta_1 \qquad (15)$$

TABLE I. FITTING PARAMETERS OF EPE20 LIFETIME MODEL

β_1	β_2	θ_1	θ_2	K
-3.581	1537	26	13	1.31×10^{10}

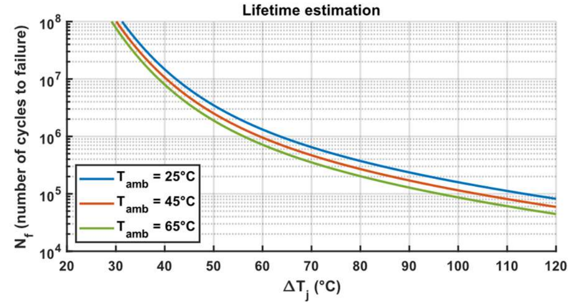

Fig. 6. Lifetime plot of semiconductor vs amplitude of temperature swing for different ambient temperatures.

B. Rainflow analysis

The temperature diagrams from the simulation test allow for an approximate determination of the thermal stresses during the cycle. In this purpose - the Rainflow algorithm can be used. The algorithm returns the number of amplitudes Rc_i within a predefined amplitude range (Fig. 7). Next, the percentage of usage for a given number of cycles $N_f(\Delta T_j)$ can be determined (Fig. 8), relative to the test conditions (Fig. 6). Fig. 7 shows that with ATC applied, high-amplitude cycles are completely reduced, while the spectrum of amplitudes is shifted toward smaller values. As shown in Fig. 8, the contribution of low temperature swings to thermal degradation is relatively insignificant. The largest contribution to semiconductor usage is made by large temperature peaks. Although there are relatively few, they cause the greatest wear of the semiconductor.

The next step is to sum up the damage for each magnitude range. The result is the percentage wear of the semiconductor during the test run. Using the proportional inverse of the percentage wear over the test duration t_{TD}, the estimated time to failure (TTF) in operating hours (or vehicle range) can be calculated:

$$TTF = \frac{t_{\mathrm{TD}}}{\sum_i \frac{Rc_i}{N_{\mathrm{f}}\left(\Delta T_{\mathrm{j}_i}\right)}} \qquad (16)$$

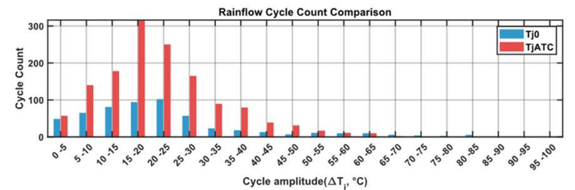

Fig. 7. Rainflow analysis for a test drive with ATC (blue) and without (red).

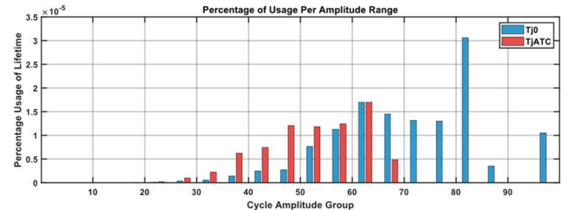

Fig. 8. Percentage of expected semiconductor usage per amplitude range.

IV. SIMULATION RESULTS ANALYSIS

Buses and trucks are commercial vehicles with high utilization, often operating 16–24 hours per day, making them more vulnerable to semiconductor wear. Therefore, simulations were performed with an example driving cycle for a heavy-duty diesel truck. Based on the cycle and the vehicle's motion equations, the required speed and external torque at a given time are modeled. This determines the voltage and current of the inverter. Semiconductor losses, and then temperature, are calculated based on the inverter's currents and voltages (Fig. 9). The parameters of the modelled vehicle are listed in Table II and the power module parameters are listed in Table III.

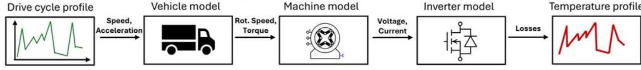

Fig. 9. Simulation setup.

TABLE II. VEHICLE PARAMETERS

Drag coeff. [-]	Front area [m²]	Mass [kg]	Wheel radius [m]	Gear ratio [-]
0.53	9.7	22000	0.5	19

TABLE III. POWER MODULE PARAMETERS

Ron [mΩ]	Rth [°C/W]	Eon [mJ]	Eoff [mJ]
2.2	0.118	0.0926 × i(t)	0.0388 × i(t)

A. Switching range influence

The frequency range is a key parameter in ATC control. Frequency adjustments are typically made within a range defined by the physical limitations of the inverter. The lower frequency limit is determined by the maximum total harmonic distortion (THD) allowed in the current of supplied machine. The upper limit of the frequency is typically set by the maximum junction temperature or by increasing electromagnetic interference (EMI) emissions and insulation exposure. In Tables IV and V, both ATC switching frequency control strategies (described in chapter III.C) are compared to the reference application without active thermal control. To ensure a fair evaluation of these methods and the reference case, the comparison was made for the same average switching frequency. This way, the average switching losses and other frequency dependent losses are also similar.

TABLE IV. LIFETIME ESTIMATION WITH METHOD A COMPARED TO REFENCE APPLICATION (WITHOUT ACTIVE THERMAL CONTROL)

Method A					**no ATC (for the same average f_{sw})**	
Swtching range [kHz]		***average f_{sw} [kHz]***	***lifetime [10^3 km]***	***Average T_j [°C]***	***lifetime [10^3 km]***	***Average T_j [°C]***
Low	***High***					
8	12	10.1	404	40.9	327	42.3
6	14	10.1	618	40.1	335	42.5
4	16	10.0	1006	39.3	338	42.2
2	18	10.0	1267	39.0	343	42.1
2	24	9.9	1267	38.9	339	42.1
2	32	10.2	1267	38.9	339	42.1

TABLE V. LIFETIME ESTIMATION WITH METHOD B COMPARED TO REFENCE APPLICATION (WITHOUT ACTIVE THERMAL CONTROL)

Method B					**no ATC (for the same average f_{sw})**	
Swtching range [kHz]		***average f_{sw} [kHz]***	***lifetime [10^3 km]***	***Average T_j [°C]***	***lifetime [10^3 km]***	***Average T_j [°C]***
Low	***High***					
2	10	9.2	1295	38.6	468	41
2	16	15.8	513	45.2	298	50.8
2	24	20.9	106	50.7	223	58.4
2	32	28.5	44	58.2	129	68.6

Both method A and method B can improve transistor lifetime compared to a system without any form of thermal control. Method A performs better with an increase in switching frequency range - as the control system has bigger capabilities. On the other hand, method B experiences a significant decrease in lifetime as the switching frequency range increases. This decline occurs because, in method B, the nominal switching frequency is always set to the maximum frequency. Shifting maximum frequency towards higher values, increases average losses and average temperature, ultimately reducing the device's lifetime. Therefore, these two methods cannot be directly compared over wider frequency control range. Method A is more adaptive, as it allows both an increase and decrease in switching frequency. This means it can respond more effectively to both rising and falling temperatures, improving system thermal stability across various operating conditions. Additionally, by centering the frequency at an optimal efficiency point, Method A achieves a better balance between overall losses and power cycling control performance across a broader range of operating conditions. However, beyond a certain point (18 kHz for the test case), further increases in the frequency range no longer provide any lifetime benefit. In fact, they may negatively impact the drive system by increasing switching losses and EMI. Therefore, in the following study, Method A was chosen as the more comprehensive approach, with a switching range of 2–18 kHz identified as optimal.

B. Estimated lifetime comparison with different lifetime models

A comparative analysis was conducted on three different semiconductor lifetime prediction models to assess the sensitivity of lifetime estimation results. In addition to the EPE20 model described earlier, CIPS08 [4] and SKiM63/93 [26] models were tested. The CIPS08 model is similar to the EPE20 model used in the previous analysis, as it employs the same formula (14), but it is not calibrated for low-temperature swings. The parameters for the EPE20 model are provided in Table I (Section III.A), while the parameters for the CIPS08 and SKiM63/93 models are listed in Tables VI and VII below.

TABLE VI. FITTING PARAMETERS OF CIPS08 LIFETIME MODEL

β_1	β_2	θ_1	θ_2	K
-3.775	1285	n/a (0)	n/a (0)	1.31×10^{10}

TABLE VII. FITTING PARAMETERS OF SKIM63/93 LIFETIME MODEL

β_1	β_2	θ_1	θ_2	K
-4.923	766	n/a (0)	n/a (0)	2.5×10^{13}

Lifetime estimations were conducted for the same temperature profile as in Table IV, incorporating method A. Results are presented in Fig. 10 and compared to the reference case (with no ATC implemented) for the same lifetime model.

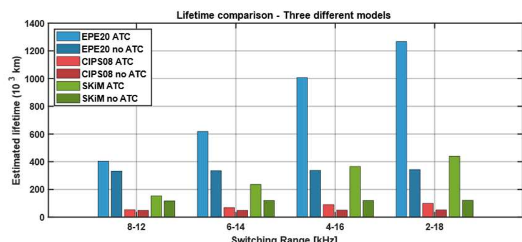

Fig. 10. Lifetime estimation (in 10^3 km) for different semiconductor models.

The three models produce significantly different results. Since lifespan depends on numerous factors, it is difficult to determine which model is the most accurate. The large difference (by an order of magnitude) between the EPE20 and CIPS08 models highlights how the model accuracy for small temperature swings drastically affects the total estimated life expectancy. However, all models show that implementing active temperature control extends the life of the semiconductor. The EPE20 and SKiM63/93 models, despite different coefficients and different estimated lifetimes, show very similar trends. For both models, implementation of ATC with a switching range of 8-12 kHz results in an increase in estimated lifetimes of about 25%, while for a switching range of 2-18 kHz there is an increase of up to 250%.

C. Temperature control range influence

Another important factor to consider when implementing ATC is the operating temperature range of active thermal control. For example, moving the ATC activation limit above 50°C, minimize unnecessary frequency changes in a range that has little impact on transistor wear. Fig. 11 summarizes the test results for various ATC temperature active ranges, evaluated using the three models presented earlier. The results are expressed in relative lifetime value, compared to a reference case with ATC active in whole temperature range. In these tests, frequency adjustments were made using Method A, within a range of 2 to 18 kHz.

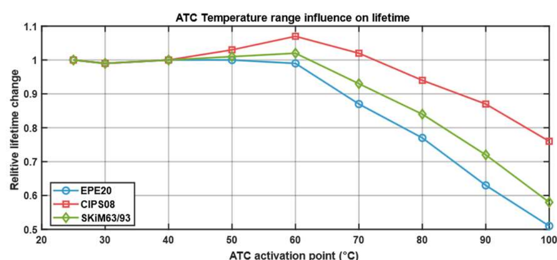

Fig. 11. Lifetime estimation for different temperature ranges (in relative values to the reference case with ATC active for whole temperature range).

Limiting excessive frequency changes at lower temperatures does not provide any significant benefit in terms of extending transistor lifespan (maximum improvement is 5% registered only for SKiM model). However, it does not have a negative impact up to approximately 50°C. Raising this limit further makes the algorithm less responsive to certain temperature spikes, ultimately reducing lifespan. This trend is consistent across all tested models. Despite this, reducing the numbers of less important frequency adjustments saves microcontroller computing resources and simplifies control system tuning by restricting its operation to a narrower temperature range. These benefits are enough to consider implementing a fixed temperature range.

D. Transient state analysis

When introducing new functionalities, it is essential to consider potential drawbacks. In the case of ATC implementation, two possible concerns arise. First, reducing the switching frequency below the nominal value may lead to increased total harmonic distortion (THD). Second, frequency increase causes higher switching losses, which increase actual temperature. Fig. 12 illustrates the acceleration of the vehicle model. During the first 0.5 seconds, the current in all three phases rises rapidly. In response to the significant increase in estimated temperature, the control system lowers the switching frequency to its minimum value (2 kHz). As a result, the initial temperature cycle reaches an amplitude of 145°C instead of 180°C. After a short time, the switching frequency gradually returns to its nominal value. Additionally, the instantaneous increase in switching frequency following the drop in current value, causes a temperature rise, which subsequently reduces the amplitude of the second cycle. A total harmonic distortion (THD) analysis was performed to assess the impact of frequency changes. In the worst-case scenario (f_{sw} = 2 kHz), the THD of the model circuit is 5.1%, whereas at the nominal switching frequency of 10 kHz, it is 1.2%.

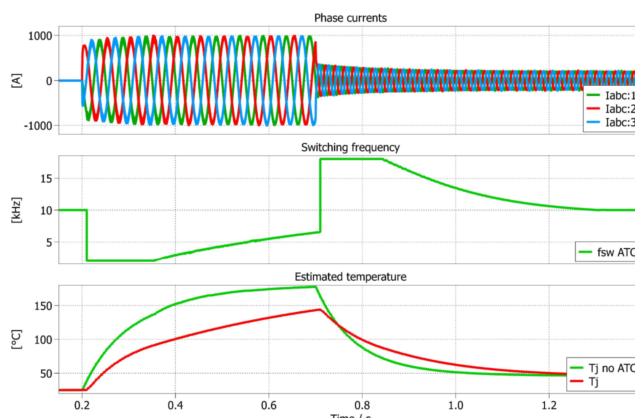

Fig. 12. Acceleration of the vehicle model – current, temperature and switching frequency adjustment during transient state.

V. CONCLUSION

The more rapid wear of the SiC semiconductors resulting from intensive thermal cycling is a non-negligible phenomenon but can be minimized at the converter control system design

stage. In applications that require long, reliable operation, implementing any form of thermal control will result in notable benefit. Even non-optimally tuned controller can extend the expected time to failure by at least 25%. Further optimizing the ATC – adjusting the frequency range and temperature threshold, the life expectancy result can be significantly improved. An optimal ATC implementation can extend the lifetime by up to three times (in terms of thermal cycling durability) compared to a system without any method of thermal control.

With active thermal control, the temperature cycle spectrum shifts towards a higher number of lower amplitude cycles, making the part of lifetime model related to low temperature swings particularly relevant. For the three tested semiconductor lifetime estimation models, the predicted operating time values can vary by up to an order of magnitude, but the scale of the benefits obtained by implementing ATC is similar. This study shows that even a simple software change, requiring no hardware changes, no additional sensors, can effectively extend semiconductor lifespan. It is important to recognize that the life expectancy estimates in this study account only for thermal stress. Other factors, such as mechanical, electrical, or humidity-induced stress, which can significantly impact overall semiconductor lifetime, have not been considered.

A preliminary analysis of ATC implementation drawbacks suggests they are minimal and shouldn't hinder adoption. A thorough investigation of the side effects of frequent changes in switching frequency on the entire drive system (both the inverter and the electrical machine) is the goal of future research. It is also planned to test the algorithm proposed in this publication on a physical device, as well as to compare two ATC methods - a software method (changing the switching frequency) and a hardware method (changing the gate resistance).

References

[1] J. Nath, Mst. F. Samad, S. P. Biswas, and Md. R. Islam, "Performance Benchmark of Three-Phase Neutral Point Clamped Inverter Using Si IGBTs, SiC MOSFETs and GaN HEMTs for Motor Drive Applications," in *2024 IEEE 34th Australasian Universities Power Engineering Conference (AUPEC)*, Sydney, Australia: IEEE, Nov. 2024, pp. 1–6. doi: 10.1109/AUPEC62273.2024.10807572.

[2] L. Ceccarelli, R. M. Kotecha, A. S. Bahman, F. Iannuzzo, and H. A. Mantooth, "Mission-Profile-Based Lifetime Prediction for a SiC mosfet Power Module Using a Multi-Step Condition-Mapping Simulation Strategy," *IEEE Trans. Power Electron.*, vol. 34, no. 10, pp. 9698–9708, Oct. 2019, doi: 10.1109/TPEL.2019.2893636.

[3] J. Kuprat, C. H. Van Der Broeck, M. Andresen, S. Kalker, M. Liserre, and R. W. De Doncker, "Research on Active Thermal Control: Actual Status and Future Trends," *IEEE J. Emerg. Sel. Top. Power Electron.*, vol. 9, no. 6, pp. 6494–6506, Dec. 2021, doi: 10.1109/JESTPE.2021.3067782.

[4] F. Hoffmann, S. Schmitt, and N. Kaminski, "Reliability of SiC MOSFET Power Modules under Consecutive H3TRB and Power Cycling Stress," *Mater. Sci. Forum*, vol. 1092, pp. 127–133, Jun. 2023, doi: 10.4028/p-3g1w6r.

[5] F. Karakaya, A. Maheshwari, A. Banerjee, J. S. Donnal, A. J. Morgan, and W. Sung, "In Situ Detection of Bond Wire Lift-Off Events in Operational SiC MOSFETs," *IEEE Trans. Power Electron.*, vol. 39, no. 12, pp. 16659–16672, Dec. 2024, doi: 10.1109/TPEL.2024.3446750.

[6] Y. Wang, Y. Ding, and Y. Yin, "Reliability of Wide Band Gap Power Electronic Semiconductor and Packaging: A Review," *Energies*, vol. 15, no. 18, p. 6670, Sep. 2022, doi: 10.3390/en15186670.

[7] H.-H. Wang, H.-C. Cheng, Y.-C. Liu, J.-Y. Syu, K.-S. Kao, and T.-C. Chang, "Solder Joint Lifetime Characterization of a SiC Power MOSFET Module Under Power Cycling," in *2024 International Conference on Electronics Packaging (ICEP)*, Toyama, Japan: IEEE, Apr. 2024, pp. 1–2. doi: 10.23919/ICEP61562.2024.10535694.

[8] Y. Shi, Y. Chen, C. Peng, W. Zhu, and H. He, "Competitive Failures Decoupling and Mechanisms Analysis of SiC MOSFET Module Under Power Cycling Stress," *IEEE J. Emerg. Sel. Top. Power Electron.*, vol. 11, no. 6, pp. 5877–5888, Dec. 2023, doi: 10.1109/JESTPE.2023.3321744.

[9] J. Chen, X. Jiang, Z. Li, H. Yu, J. Wang, and Z. J. Shen, "Investigation on Effects of Thermal Stress on SiC MOSFET Degradation through Power Cycling Tests," in *2020 IEEE Applied Power Electronics Conference and Exposition (APEC)*, New Orleans, LA, USA: IEEE, Mar. 2020, pp. 1106–1110. doi: 10.1109/APEC39645.2020.9124249.

[10] Z. Ni, X. Lyu, O. P. Yadav, B. N. Singh, S. Zheng, and D. Cao, "Overview of Real-Time Lifetime Prediction and Extension for SiC Power Converters," *IEEE Trans. Power Electron.*, vol. 35, no. 8, pp. 7765–7794, Aug. 2020, doi: 10.1109/TPEL.2019.2962503.

[11] P. Naveen and P. Ms.Hema Rani, "Reliability Improvement of IGBT Employed in Boost Converter using Active Thermal Control," in *2021 International Conference on Intelligent Technologies (CONIT)*, Hubli, India: IEEE, Jun. 2021, pp. 1–6. doi: 10.1109/CONIT51480.2021.9498456.

[12] D. A. Murdock, J. E. R. Torres, J. J. Connors, and R. D. Lorenz, "Active thermal control of power electronic modules," *IEEE Trans. Ind. Appl.*, vol. 42, no. 2, pp. 552–558, Mar. 2006, doi: 10.1109/TIA.2005.863905.

[13] *Proceedings of PCIM Europe 2015: International Exhibition and Conference for Power Electronics, Intelligent Motion, Renewable Energy and Energy Management: 19-20 May 2015.* Piscataway, NJ: IEEE, 2015.

[14] A. Griffo, J. Wang, K. Colombage, and T. Kamel, "Real-Time Measurement of Temperature Sensitive Electrical Parameters in SiC Power MOSFETs," *IEEE Trans. Ind. Electron.*, vol. 65, no. 3, pp. 2663–2671, Mar. 2018, doi: 10.1109/TIE.2017.2739687.

[15] A. Acquaviva, A. Rodionov, A. Kersten, T. Thiringer, and Y. Liu, "Analytical Conduction Loss Calculation of a MOSFET Three-Phase Inverter Accounting for the Reverse Conduction and the Blanking Time," *IEEE Trans. Ind. Electron.*, vol. 68, no. 8, pp. 6682–6691, Aug. 2021, doi: 10.1109/TIE.2020.3003586.

[16] A. Kahwa, H. Obara, and Y. Fujimoto, "Estimation and Analysis of Power Loss in a Reduced Switches Count H-Bridge Multilevel Inverter," in *2019 IEEE International Conference on Mechatronics (ICM)*, Ilmenau, Germany: IEEE, Mar. 2019, pp. 25–30. doi: 10.1109/ICMECH.2019.8722859.

[17] Z. Zhou, P. M. Holland, and P. Igic, "Compact thermal model of a three-phase IGBT inverter power module," in *2008 26th International Conference on Microelectronics*, Nis, Serbia and Montenegro: IEEE, May 2008, pp. 167–170. doi: 10.1109/ICMEL.2008.4559249.

[18] S. C. Rangari, H. M. Suryawanshi, and B. Shah, "Effect of inverter switching frequency on the stator current harmonics of five phase induction motor," in *2017 International Conference on Energy, Communication, Data Analytics and Soft Computing (ICECDS)*, Chennai: IEEE, Aug. 2017, pp. 2128–2132. doi: 10.1109/ICECDS.2017.8389826.

[19] P. Karlovsky and J. Lettl, "Influence of switching frequency on torque ripples in model predictive control of induction motor drive," in *2017 9th International Conference on Electronics, Computers and Artificial Intelligence (ECAI)*, Targoviste: IEEE, Jun. 2017, pp. 1–4. doi: 10.1109/ECAI.2017.8166398.

[20] M. Van Der Geest, H. Polinder, and J. A. Ferreira, "Influence of PWM switching frequency on the losses in PM machines," in *2014 International Conference on Electrical Machines (ICEM)*, Berlin, Germany: IEEE, Sep. 2014, pp. 1243–1247. doi: 10.1109/ICELMACH.2014.6960341.

[21] C. Barbagallo, S. A. Rizzo, G. Scelba, G. Scarcella, and M. Cacciato, "On the Lifetime Estimation of SiC Power MOSFETs for Motor Drive Applications," *Electronics*, vol. 10, no. 3, p. 324, Jan. 2021, doi: 10.3390/electronics10030324.

[22] Y. Zhong, X. He, Z. Wang, J. Luo, B. Wang, and Q. Li, "Review of HTRB and HTGB Reliability of SiC MOSFETs," in *2024 7th International Conference on Energy, Electrical and Power Engineering (CEEPE)*, Yangzhou, China: IEEE, Apr. 2024, pp. 1161–1168. doi: 10.1109/CEEPE62022.2024.10586507.

[23] T. Zhou *et al.*, "Experimental and Theoretical Study on failure mechanism of Superjunction MOSFET under H3TRB Testing," in *2024 36th International Symposium on Power Semiconductor Devices and ICs (ISPSD)*, Bremen, Germany: IEEE, Jun. 2024, pp. 554–557. doi: 10.1109/ISPSD59661.2024.10579610.

[24] Z. Zheng, L. Meng, X. Li, B. Ruan, and H. Cui, "Analysis of Power Cycle Aging Test for SiC MOSFET," in *2023 Global Reliability and Prognostics and Health Management Conference (PHM-Hangzhou)*, Hangzhou, China: IEEE, Oct. 2023, pp. 1–5. doi: 10.1109/PHM-Hangzhou58797.2023.10482448.

[25] F. Hoffmann, S. Schmitt, and N. Kaminski, "Lifetime Modeling of SiC MOSFET Power Modules During Power Cycling Tests at Low Temperature Swings," in *2023 35th International Symposium on Power Semiconductor Devices and ICs (ISPSD)*, Hong Kong: IEEE, May 2023, pp. 294–297. doi: 10.1109/ISPSD57135.2023.10147533.

[26] R. Schmidt, P. Newman, and U. Scheuermann, "Power cycling testing with different load pulse durations," in *7th IET International Conference on Power Electronics, Machines and Drives (PEMD 2014)*, Manchester, UK: Institution of Engineering and Technology, 2014, p. 1.9.03-1.9.03. doi: 10.1049/cp.2014.0475.